

ADDITIONAL RESULTS ON SPACE ENVIRONMENTAL EFFECTS ON  
POLYMER MATRIX COMPOSITES — EXPERIMENT AO180

R. C. Tennyson  
University of Toronto Institute for Aerospace Studies  
Toronto, Ontario, Canada  
M3H 5T6

ABSTRACT

This report presents additional experimental results on the atomic oxygen erosion of boron, Kevlar® and graphite fiber reinforced epoxy matrix composites. Damage of composite laminates due to micrometeoroid /debris impacts is also examined with particular emphasis on the relationship between damage area and actual hole size due to particle penetration. Special attention is given to one micrometeoroid impact on an aluminum base plate which resulted in ejecta visible on an adjoining vertical flange structure.

EROSION OF POLYMER MATRIX COMPOSITES

Experiment AO180 was located at station D-12 on LDEF, about 82° relative to its velocity vector. NASA estimates the atomic oxygen (AO) fluence at  $\sim 1.2 \times 10^{21}$  atoms/cm<sup>2</sup> and the total equivalent sun hours of VUV radiation at  $\sim 6900$  hours. It should be noted that the erosion data presented may well result from combined AO/VUV exposure. However, at the present time, the possible synergistic effects cannot be separated.

BORON/EPOXY LAMINATES (SP-290)

The erosion of boron/epoxy laminates was restricted to the outer epoxy layer. Figure 1 shows a comparison of the unexposed (a) and exposed (b) areas, where it is evident that loss of the outer epoxy layer reveals the woven glass fiber cloth (used as a binder material) and the unidirectional boron (coating over tungsten) fibers. Cross-sectional views (Figure 2) show the outer resin layer, glass fibers and composition of the reinforcing 'boron' fiber with its tungsten core. Figure 3 presents a similar view including the AO erosion profiles of the epoxy layer. For a tube structure, the erosion angle varies with circumferential position around the tube, as demonstrated by the results plotted in Figure 4. Finally, close-up examination of the boron fibers exposed to AO reveals a grain structure (Figure 5) that has formed in the boron coating, although no loss of boron material due to erosion was observed. The combination of boron reinforcing fibers overlaid with glass fiber scrim cloth yields a laminate that is significantly less sensitive to AO erosion than graphite and Kevlar® reinforcements.

## KEVLAR®/EPOXY LAMINATES (SP-328)

Kevlar®/epoxy flat plate laminates were mounted on the exterior of the UTIAS LDEF experiment. The schematic shown in Figure 6 illustrates a shadow region (A) adjacent to an aluminum (Al) end tab, the outer exposed face (B) and erosion areas (C) on the bottom face (D) which resulted from AO reflection off cylindrical aluminum end fixtures mounted on adjacent tube specimens. Figure 7 presents SEM photographs of two unexposed regions, A and D. These can be compared to the AO erosion surface morphologies found in the exposed areas, B and C. The fibrous nature of the eroded Kevlar® is clearly evident in B, with C more typical of non-directional AO attack on the outer resin layer. Note the difference in texture of the Kevlar® fibers between B and C. In photograph B, the outer epoxy layer is gone and only the partially eroded Kevlar® fibers in the first layer remain.

## GRAPHITE/EPOXY LAMINATES

The surface erosion morphology observed on graphite/epoxy laminates due to AO is shown in Figure 8 for a 90°, 4 ply tube (934/T300). When viewing the cross-section of a laminate, one finds that the AO fluence at station D-12 was sufficient to erode the outer epoxy layer and a portion of the reinforcing graphite fibers. Figure 9 presents SEM photographs of unexposed and exposed regions for a ( $\pm 43^\circ$ )<sub>4s</sub> tube (SP288/T300). Erosion of the graphite fibers is clearly evident.

XPS measurements have also been made on the surface composition of a graphite/epoxy flat plate laminate (934/T300).\* Comparing "unexposed" with "exposed" surface data (Table I), it is interesting to note a substantial reduction in the C-O content and a large increase in the O composition on the exposed surface. Furthermore, the exposed region also exhibits a large increase in the Si content, probably due to contamination.

TABLE I. APPROXIMATE ATOM % SURFACE COMPOSITION OF GRAPHITE/EPOXY COMPOSITE (934/T300) FROM LDEF AS MEASURED BY XPS

Sample	C			O	N	Na	Si	S
	C=O	C-O	CH					
Unexposed								
#1	5.8	19.0	41.3	23.3	4.4	0.4	3.6	2.2
#2	6.7	16.0	41.8	25.7	3.8	0.5	4.3	1.2
Exposed								
#1	4.6	6.2	38.9	34.0	1.8	0.5	13.0	0.9
#2	4.0	6.6	42.1	32.1	1.7	0.9	11.8	0.6

Courtesy: T. Wittberg, Research Institute  
Nonmetallic Materials Division  
University of Dayton

\* Courtesy of T. Wittberg, Research Institute, Nonmetallic Materials Division, University of Dayton.

## MICROMETEOROID/DEBRIS IMPACTS

### Micrometeoroid Impact on Aluminum Support Structure

The largest impact found on experiment AO180 occurred on an aluminum base plate, with an ejecta splash observed on an adjacent flange structure (Figure 10). A view of the 1 mm diameter crater is shown in Figure 11. EDS spectra of the crater rim material composition (Figure 12) exhibits a strong Fe peak along with the Al substrate. Based on this evidence it is assumed that the crater resulted from a micrometeoroid impact. Figure 13 contains a SEM photograph of the surface ejecta splash pattern on the flange structure. Details of the different splash patterns in this region are shown in Figure 14. An aluminum ejecta particle, visible in Figure 14, is enlarged in Figure 15 and Figure 16 (lower photograph). Figure 16 presents two different forms of aluminum ejecta particles and their associated splash patterns. The lower photograph shows the remnants of a molten particle while the upper photograph shows the full spherical form of an aluminum particle.

### Impact Damage on Composite Laminates

Micrometeoroid/debris impacts on polymer matrix composites do not produce the typical hemispherical craters found on metallic structures. Rather, because of the brittle nature of the resin matrix, one generally finds penetration holes with adjacent surface damage, some internal ply delamination and local fiber fractures. For brittle fibers such as graphite, the impact and exit holes exhibit brittle fiber fractures such as shown in Figure 17. On the other hand, tough non-brittle fibers such as aramid fail in a "brush or broom" mode surrounding the impact damage region. Figure 18 presents four impacts on a single Kevlar®/epoxy tube [SP-328, ( $\pm 45$ )<sub>4s</sub>]. Enlargements of the damage areas are given in Figure 19 where it can be seen that three penetrations occurred with one grazing (or low energy) impact that produced only local surface damage. Note the fiber failure mode in photo 4. From the enlargements, it was possible to scan the images to calculate the surface damage area and impact hole size. Using an image enhancement backlighting technique that works well on translucent materials, one can also estimate the penetration depth of the impacting particle. Figure 20 presents the images and data obtained for these four impact sites. At this point in time, only 10 impact sites (out of 84) have been found on the composite samples, a summary of which is given in Table II with estimates of surface damage area, hole size and penetration. Such data will be useful for estimating total damage on composite structures that arises from micrometeoroids/debris.

TABLE II. SUMMARY OF IMPACT FEATURES ON COMPOSITE SPECIMENS  
(EXPERIMENT AO 180)

Material Type	Sample Type	Number of Plies	Sample No.	Surface Damage Area (mm <sup>2</sup> )	Hole Area (mm <sup>2</sup> )	Particle Penetration Depth (Number of plies)
Graphite/Epoxy (T300/5208)	Plate	4		0.222	0.222	>4
Graphite/Epoxy (SP 288/T300)	Tube	4	1T10	1.064	0.083	>4
Aramid* Fiber/Epoxy (SP 328)	Tube	4	2T2	1.162	0.036	1 - 2
"	Tube	4	2T4	0.498	0.015	-1
"	Tube	4	2T11	0.423	0.018	-1
"	Tube	4	2T16	1.253	0.076	2 - 3
"	Tube	4	2T17(1)	0.223	—	1 - 2
			2T17(2)	1.445	0.033	2 - 3
			2T17(3)	0.370	—	-1
			2T17(4)	0.881	0.020	2 - 3

\*Kevlar

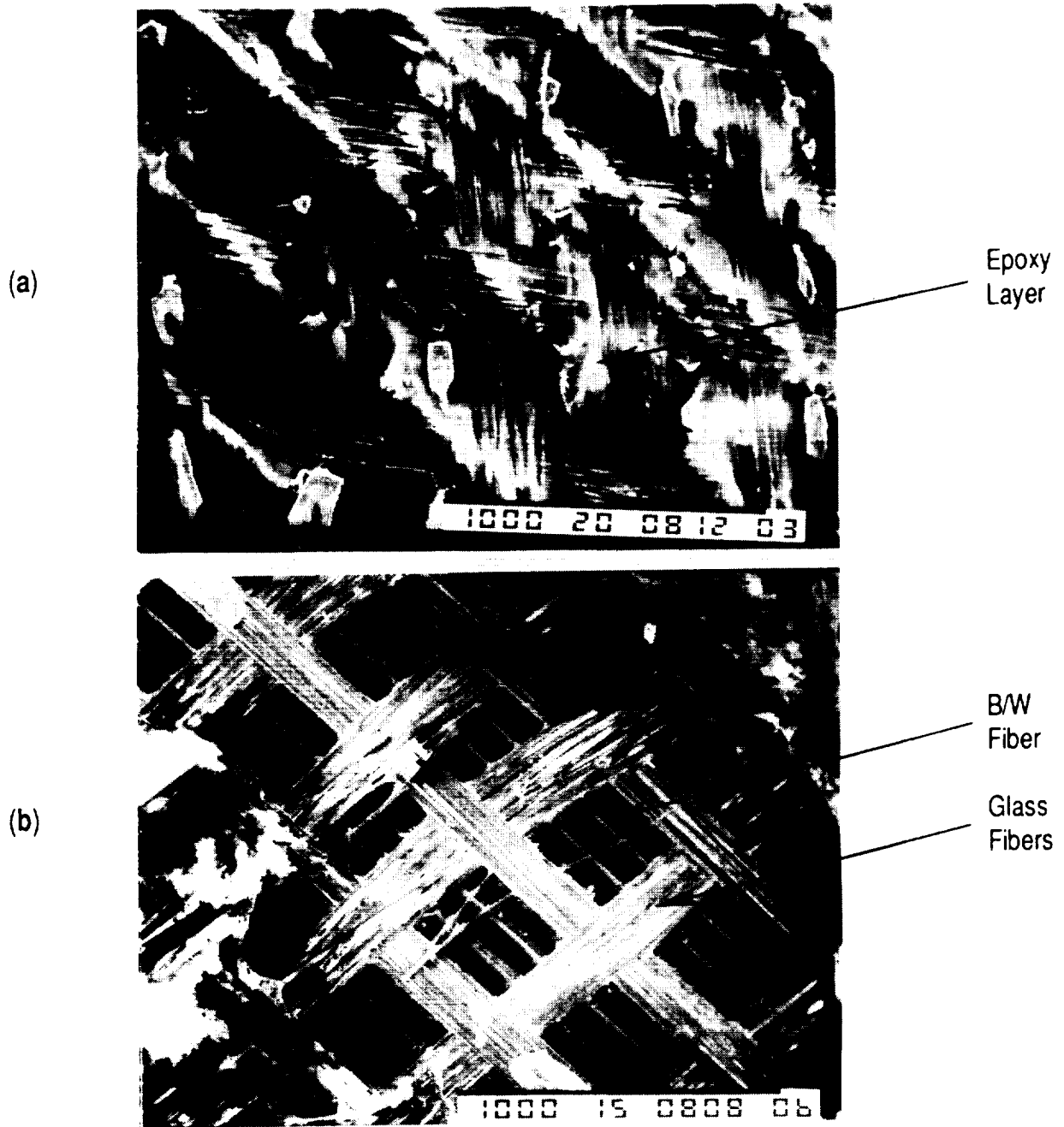
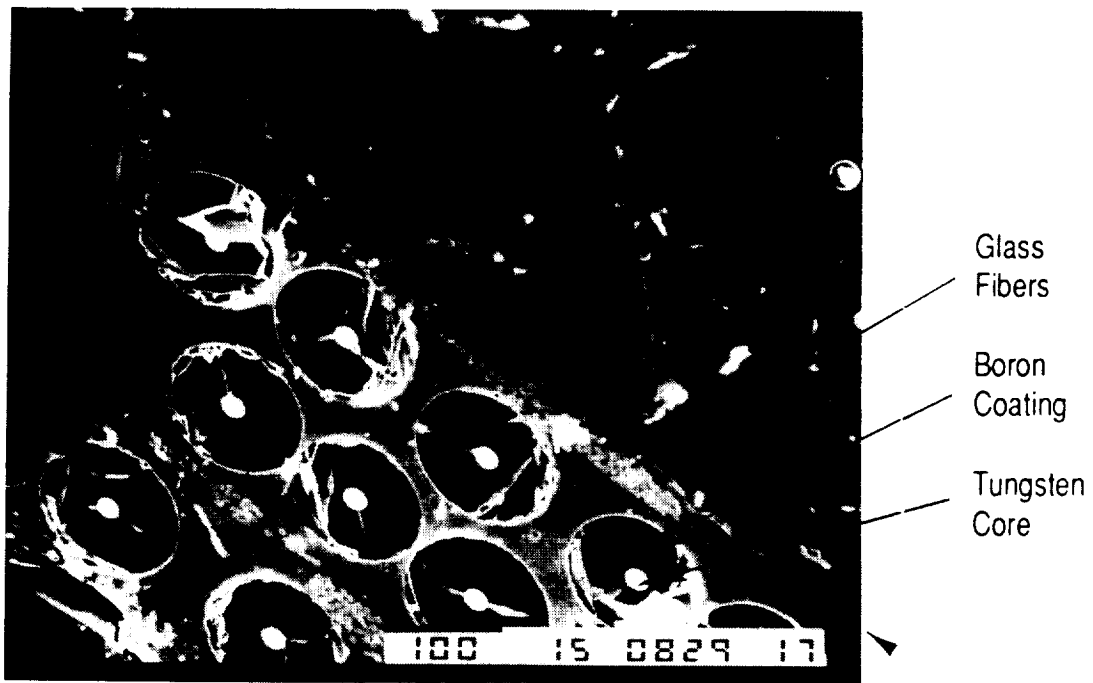
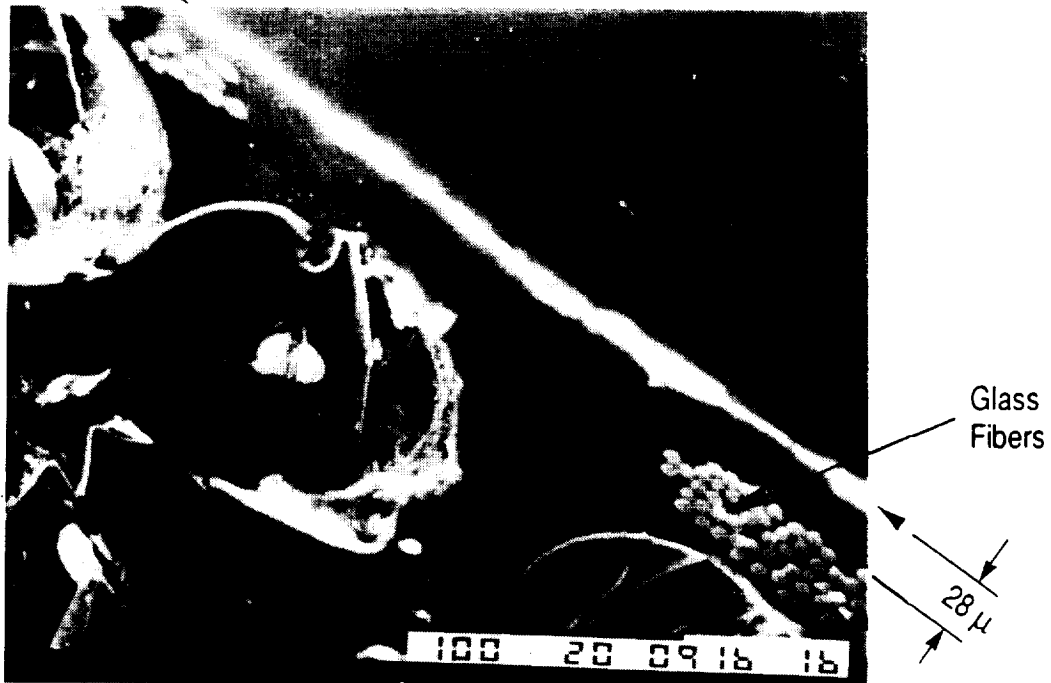


Fig. 1 SEM Photographs of Boron/Epoxy Tube Surface [SP-290,  $(\pm 45^\circ)_4S$ ] (a) Unexposed (x50), (b) Exposed to Atomic Oxygen (x50)



(x150)



(x350)

Fig. 2 SEM Photographs of Cross-Section of Unexposed Boron/Epoxy Tube [SP-290,  $(\pm 45^\circ)_4S$ ]. (Arrows delineate boundary between outer epoxy layer and potting compound)

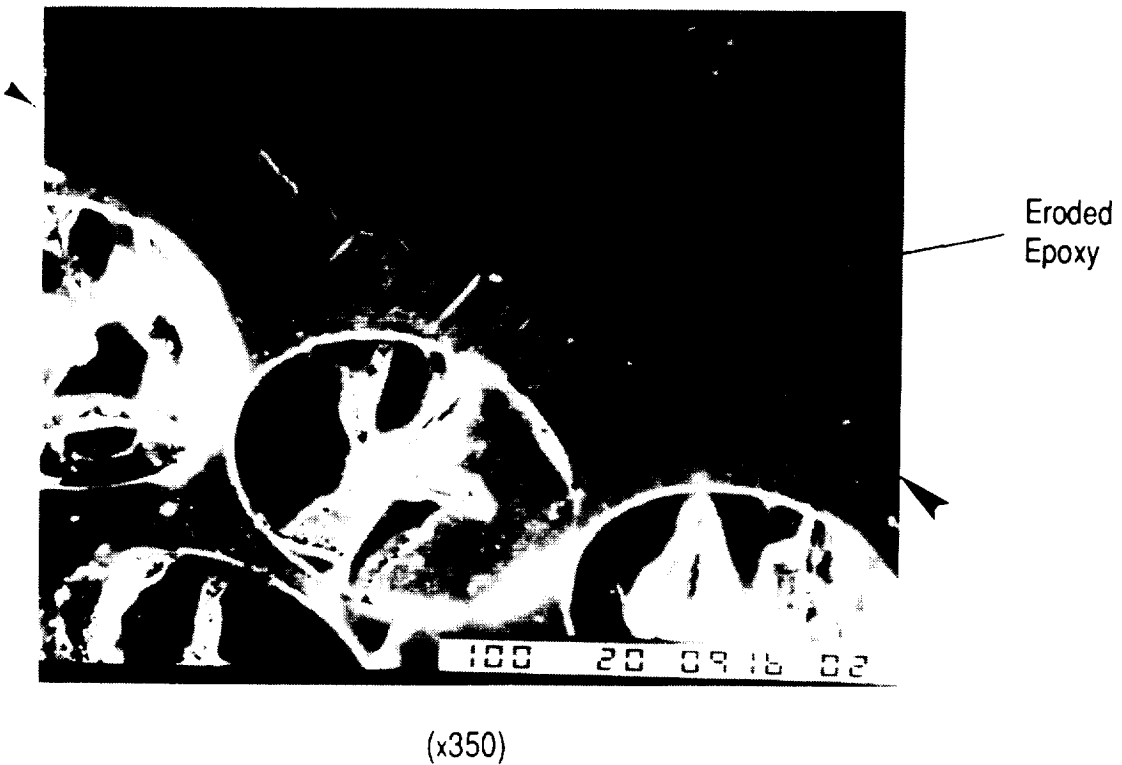
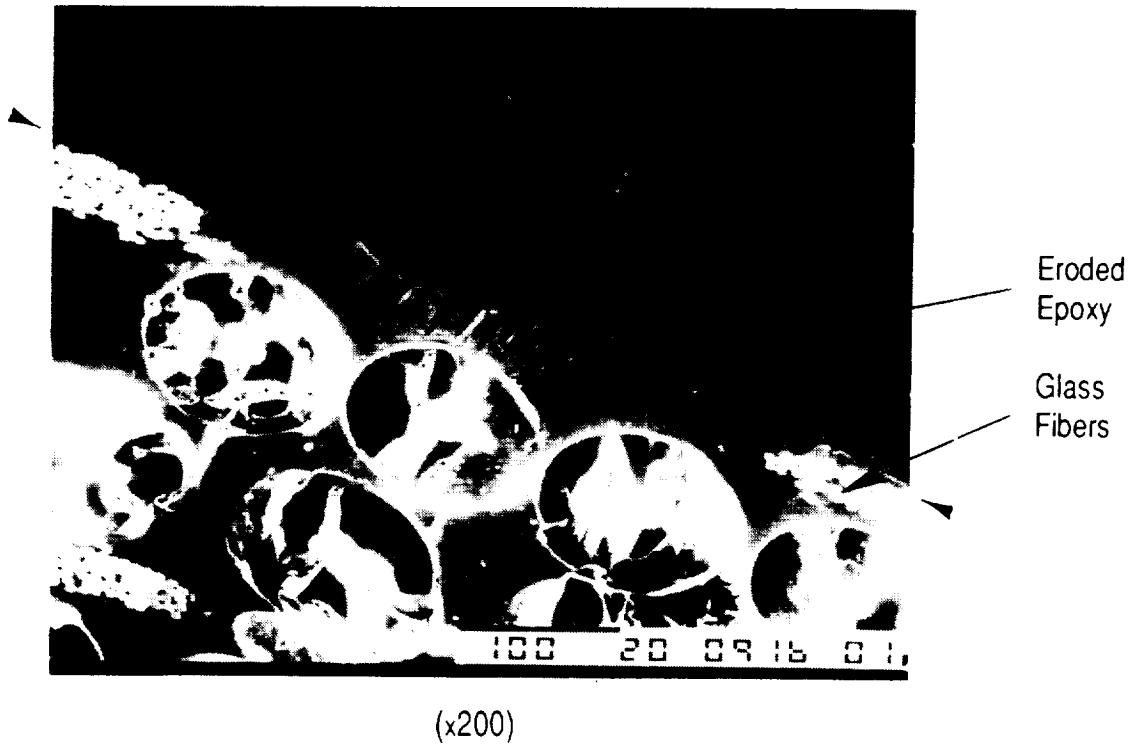


Fig. 3 SEM Photographs of Eroded Cross-Section of Boron/Epoxy Tube [SP-290, ( $\pm 45^\circ$ )<sub>4S</sub>] Exposed to Atomic Oxygen. (Arrows delineate boundary between outer epoxy layer and potting compound)

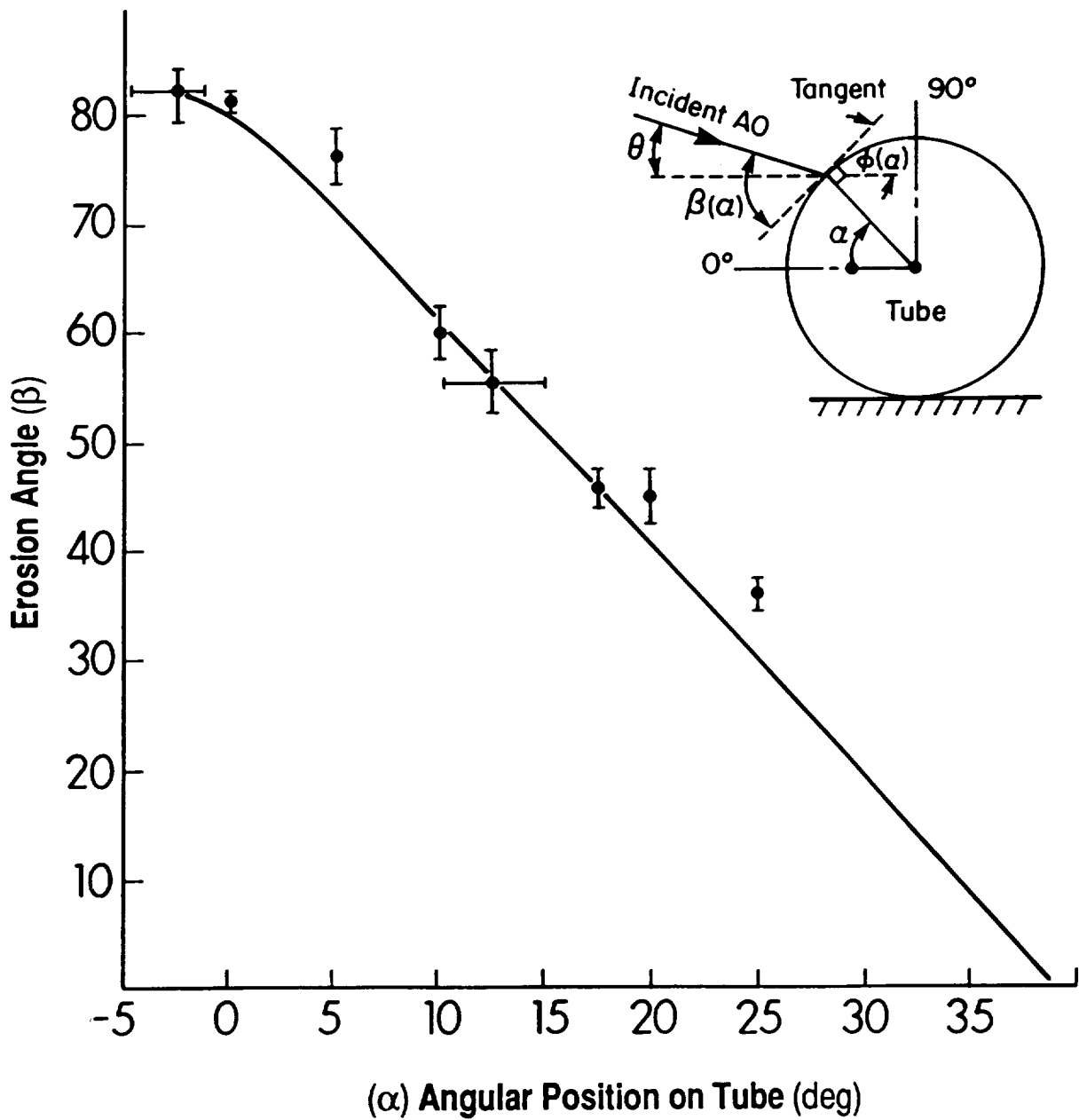


Fig. 4 Variation in Erosion Angle ( $\beta$ ) with Angular Position ( $\alpha$ ) around Boron/Epoxy Tube [SP-290, ( $\pm 45^\circ$ )<sub>4S</sub>]

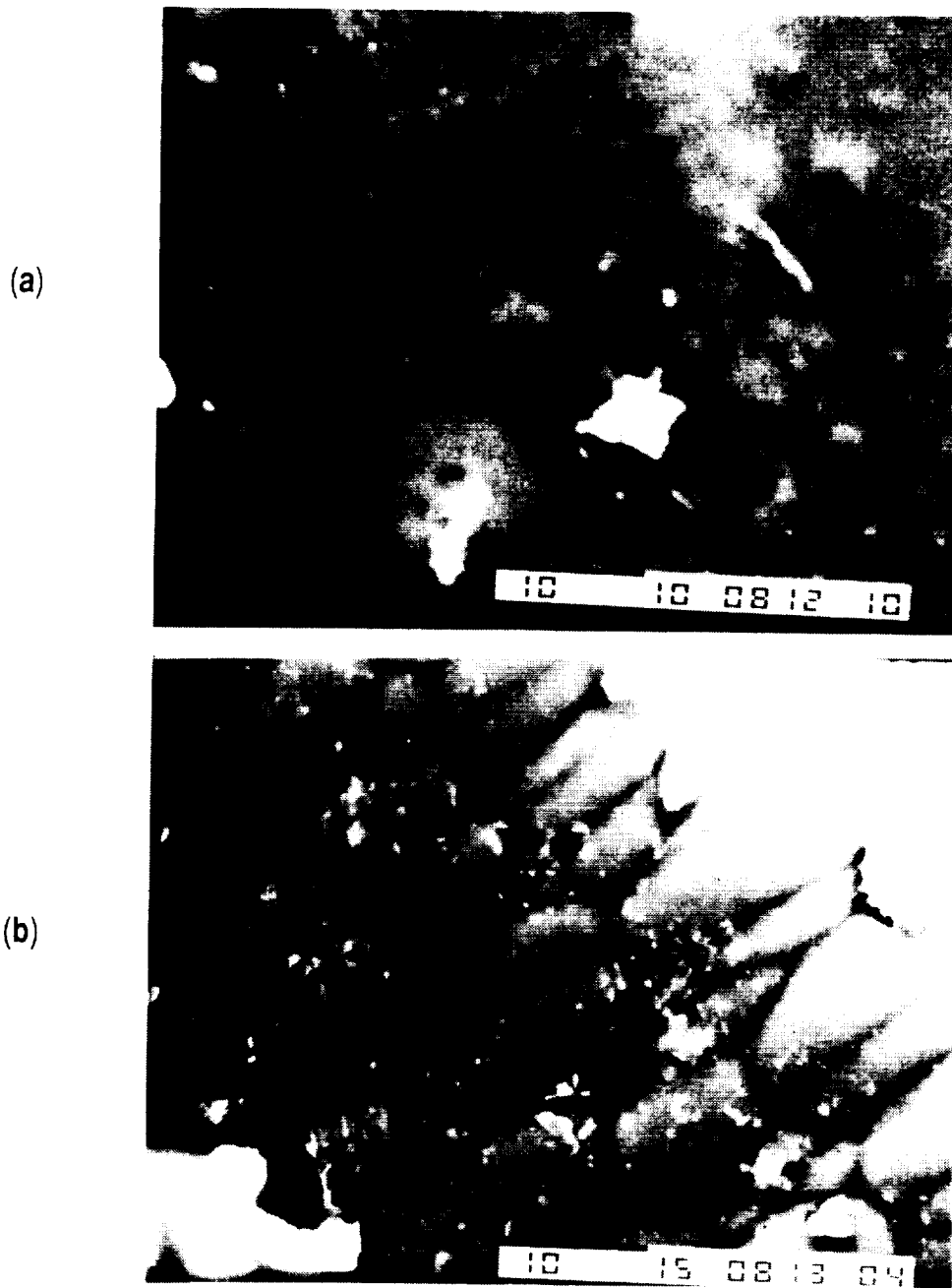


Fig. 5 SEM Photographs of the surface texture of a B/W fiber in a Boron/Epoxy Tube [SP-290,  $(\pm 45^\circ)_4S$ ] (a) Unexposed (x2000), (b) Exposed to Atomic Oxygen (x2000)

ORIGINAL PAGE  
BLACK AND WHITE PHOTOGRAPH

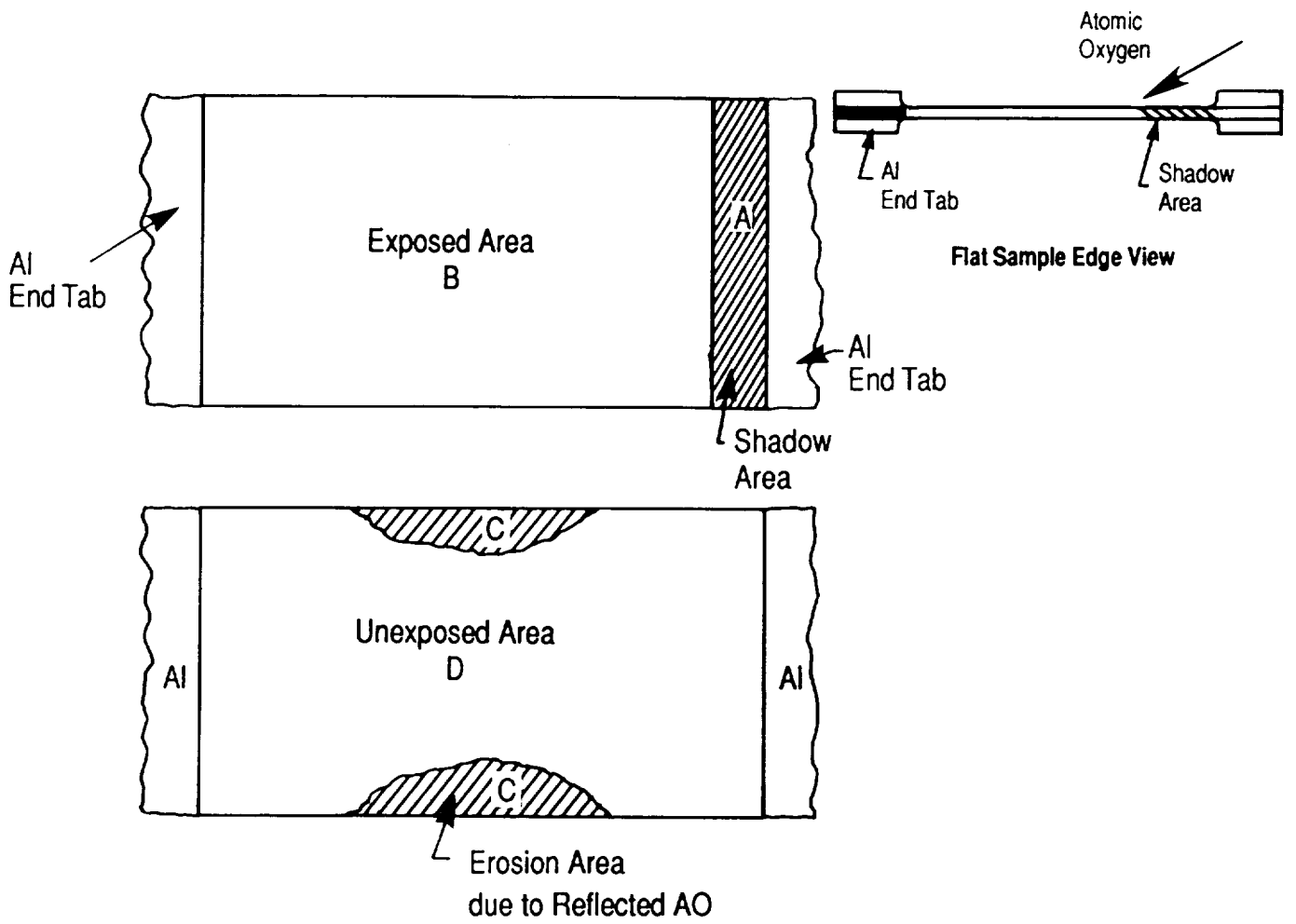


Fig. 6 Kevlar®/Epoxy (SP-328) Flat Plate Laminate



Exposed Area B (x750)



Erosion Area C (x750)



Shadow Area A (x50)



Unexposed Area D (x50)

Fig. 7 SEM Photographs of Kevlar®/Epoxy Laminate [SP-328, ( $\pm 43^\circ$ )<sub>4S</sub>]

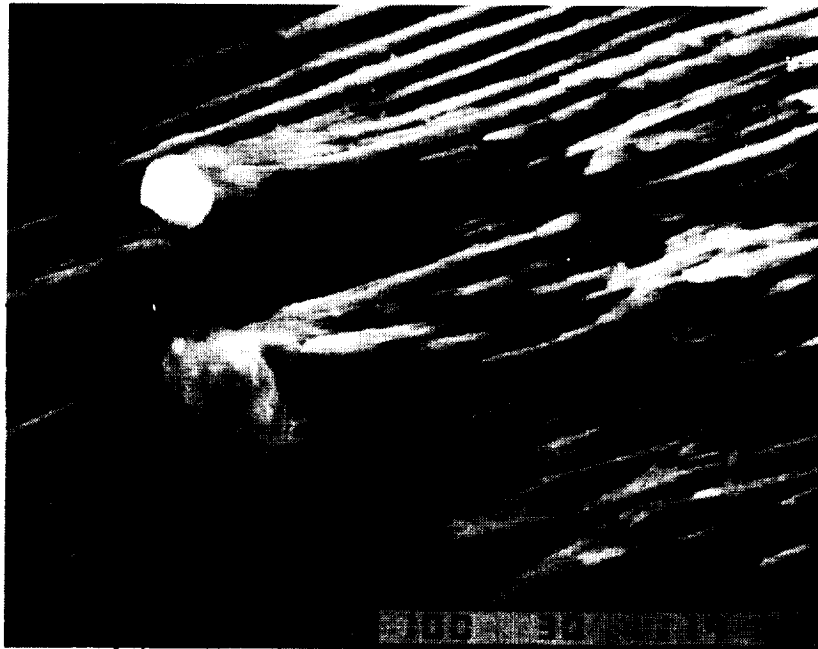


Fig. 8 SEM Photograph of Surface Morphology on Exposed Graphite/Epoxy Tube [934/T300, (90°)<sub>4S</sub>]

ORIGINAL PAGE  
BLACK AND WHITE PHOTOGRAPH

ORIGINAL PAGE  
BLACK AND WHITE PHOTOGRAPH

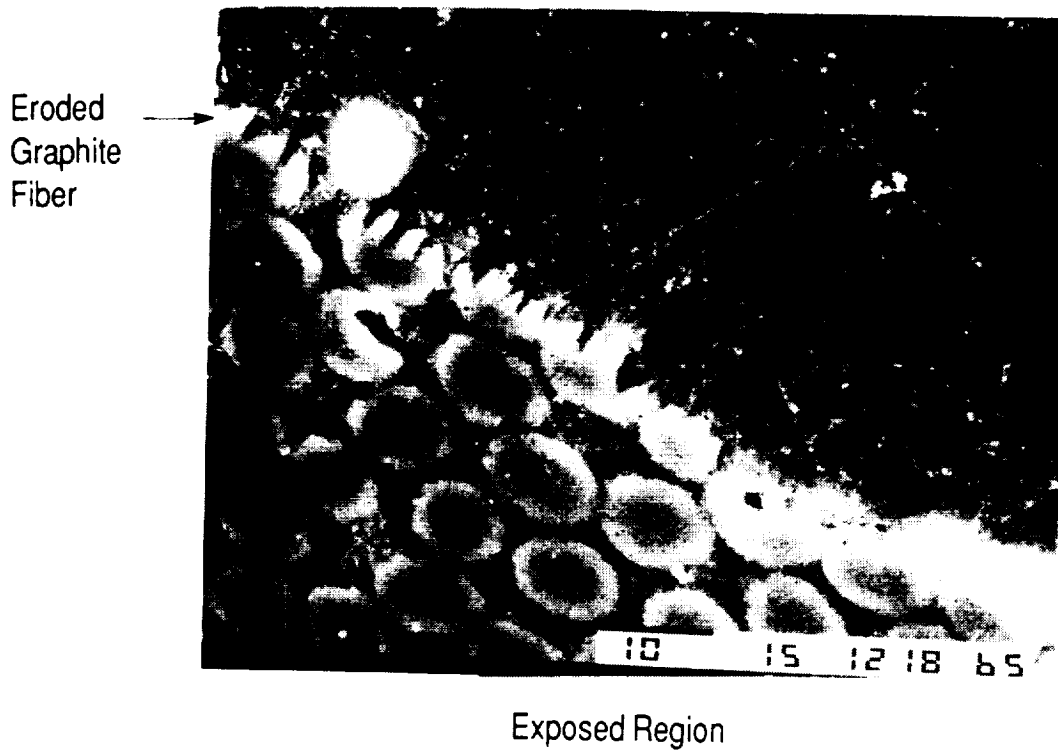
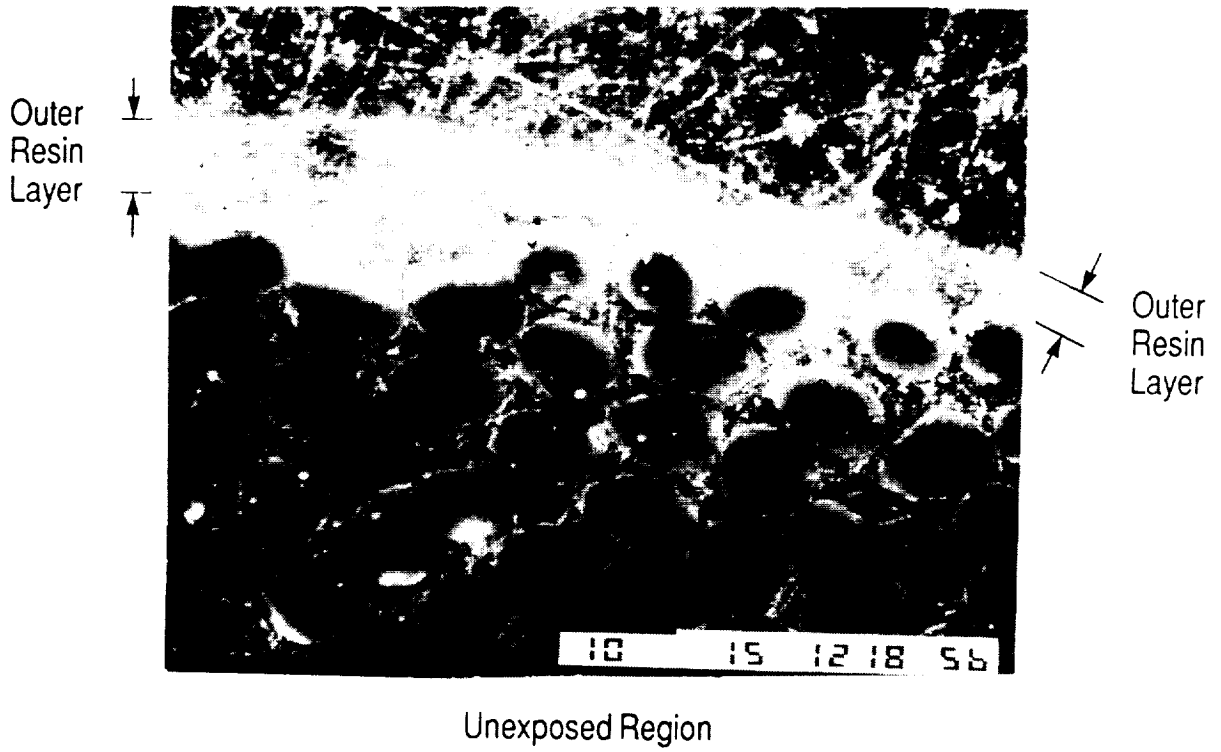


Fig. 9 SEM Cross-Sectional Photographs of Graphite/Epoxy Tube Subjected to AO Erosion [SP-288/T300, ( $\pm 43^\circ$ )<sub>4S</sub>]

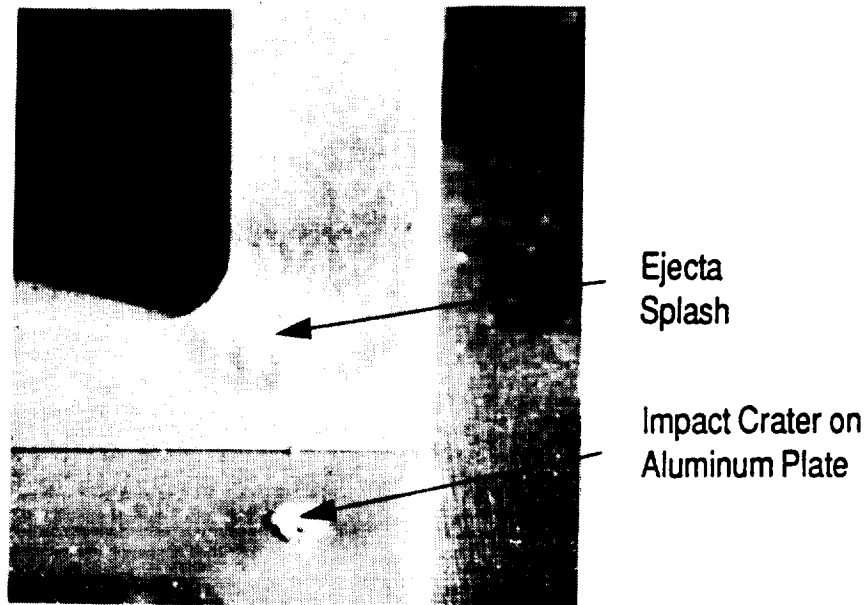


Fig. 10 View of Micrometeoroid Impact Crater and Ejecta Splash Pattern on Adjacent Vertical Flange Structure

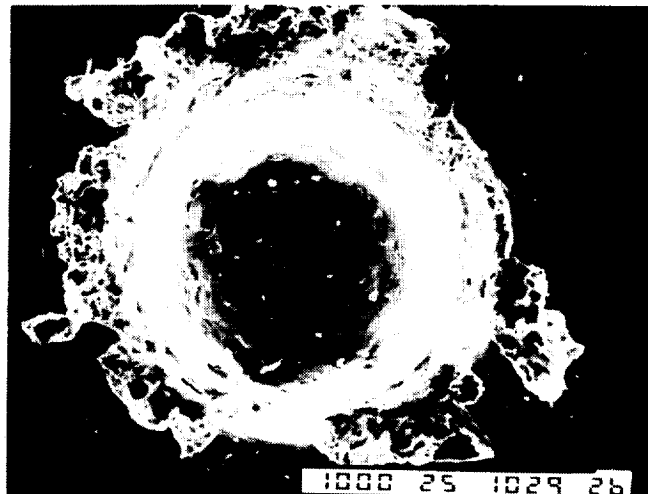
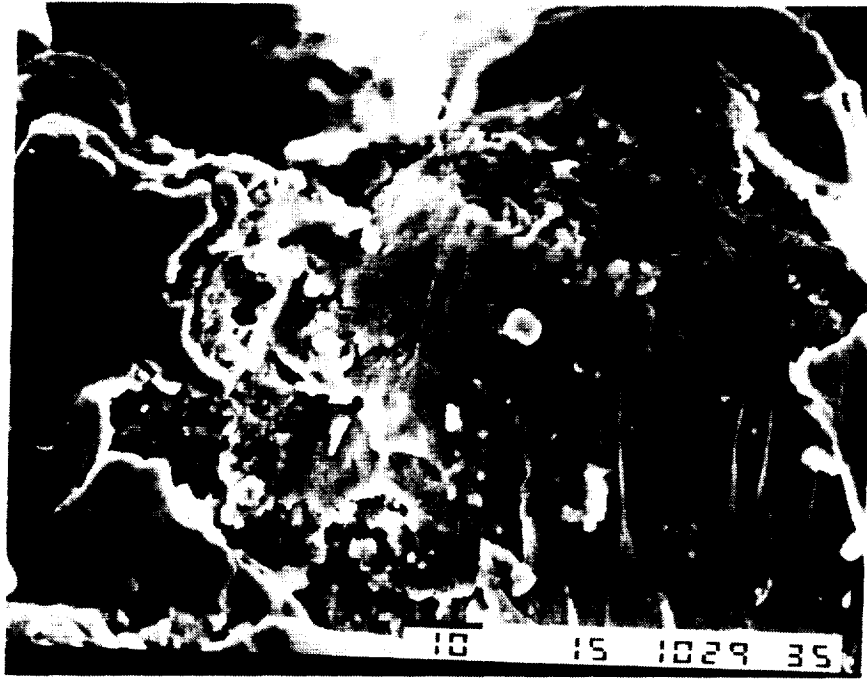


Fig. 11 View of Micrometeoroid Crater on Aluminum Base Plate



Crater  
Rim  
Ejecta

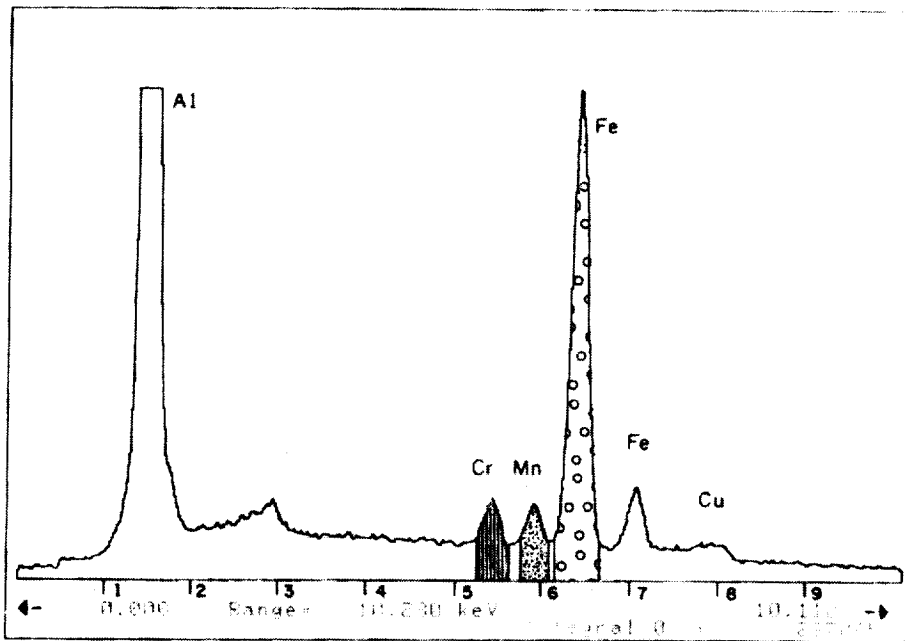


Fig. 12 Crater Ejecta and Elemental Composition (EDS Spectra)

ORIGINAL PAGE  
BLACK AND WHITE PHOTOGRAPH

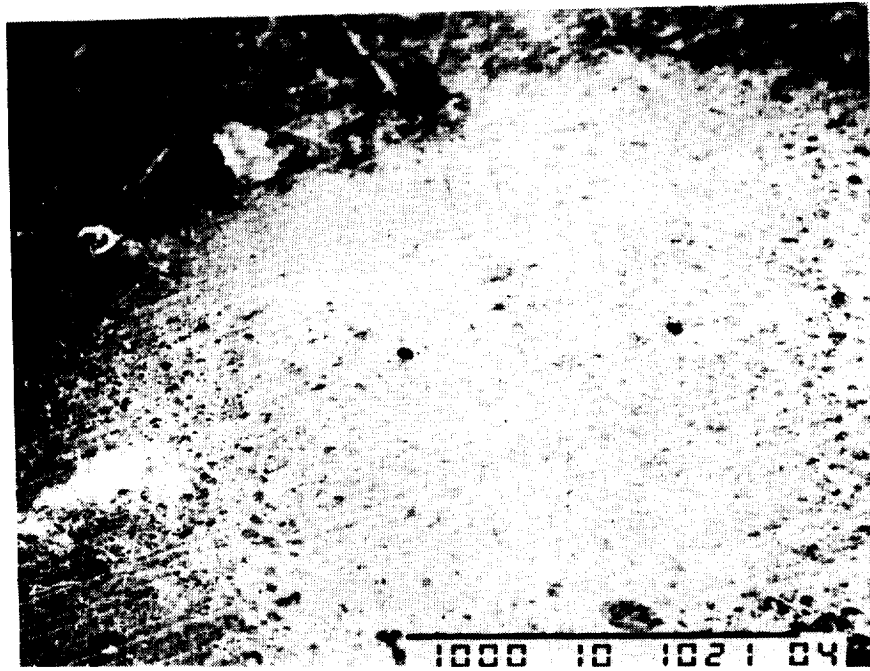
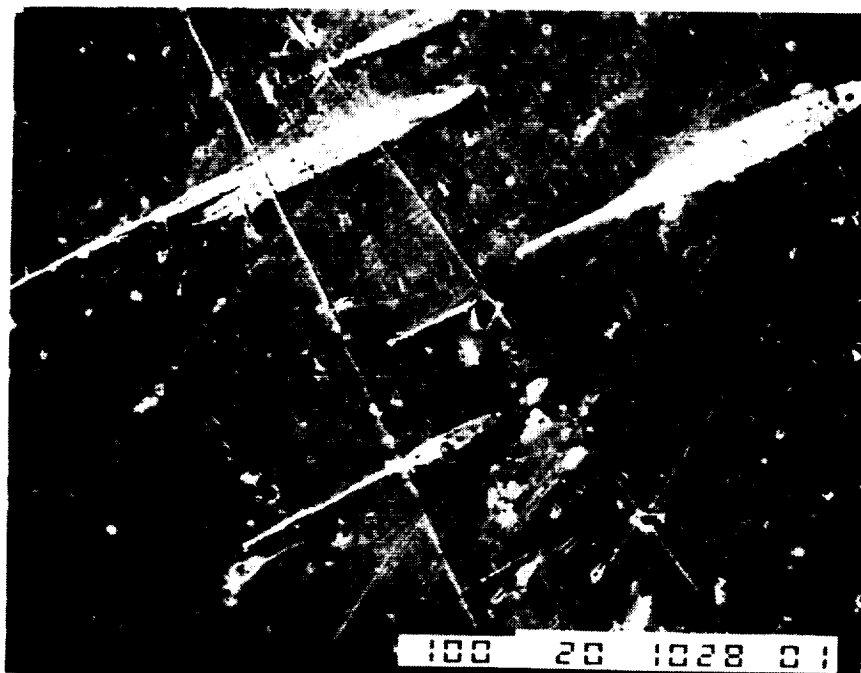
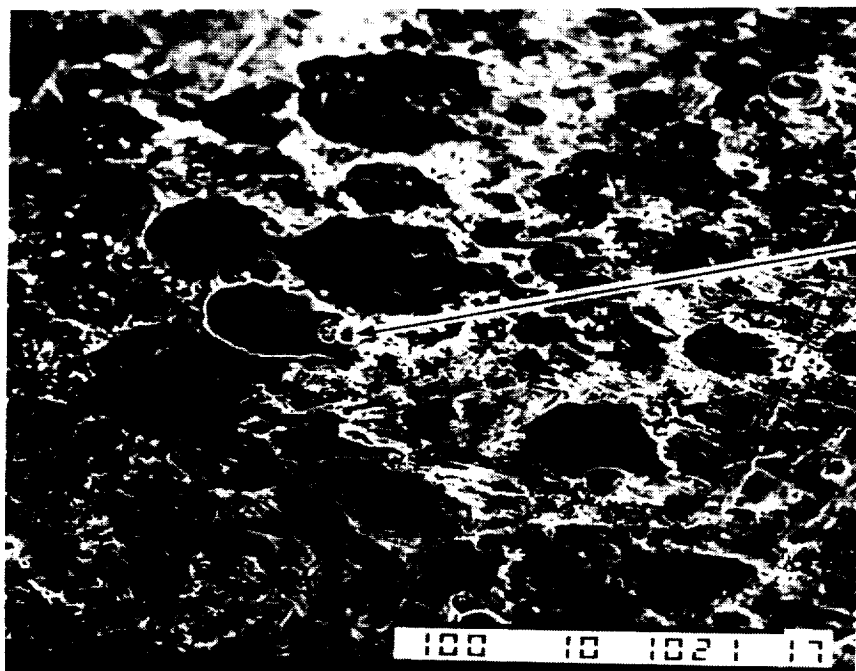


Fig. 13 Ejecta Splash Pattern on Vertical Flange Structure Adjacent to Crater

ORIGINAL PAGE  
BLACK AND WHITE PHOTOGRAPH



Splash  
Pattern



Al Particle and its  
Splash Pattern

Fig. 14 Different Splash Patterns formed by Ejecta from Micrometeoroid Impact

ORIGINAL PAGE  
BLACK AND WHITE PHOTOGRAPH

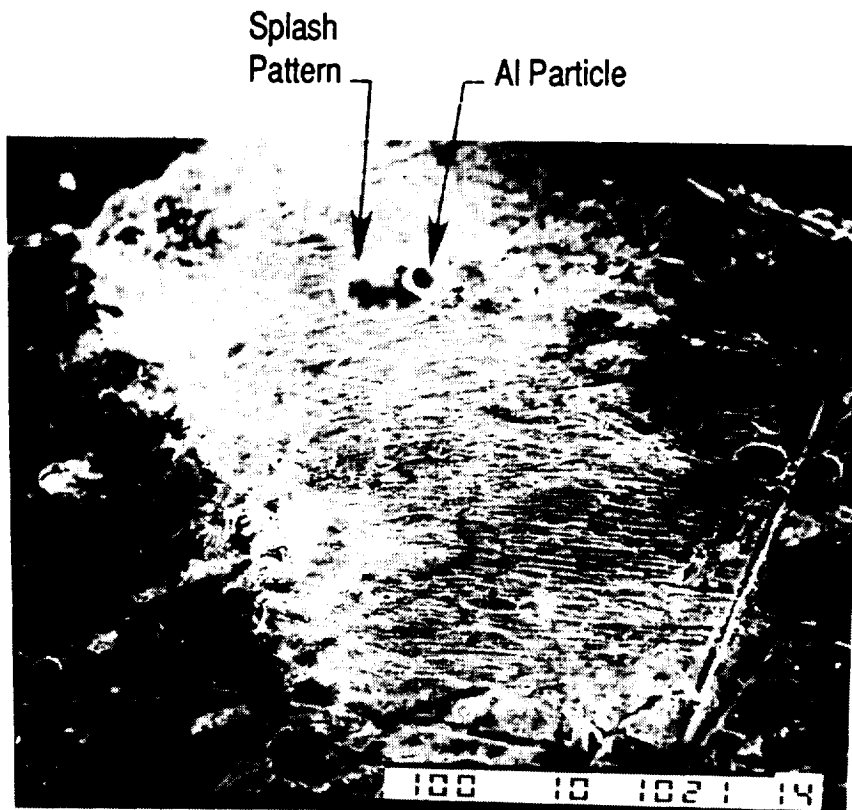


Fig. 15 Superposition of Aluminum Ejecta Particle on Splash Pattern

ORIGINAL PAGE  
BLACK AND WHITE PHOTOGRAPH

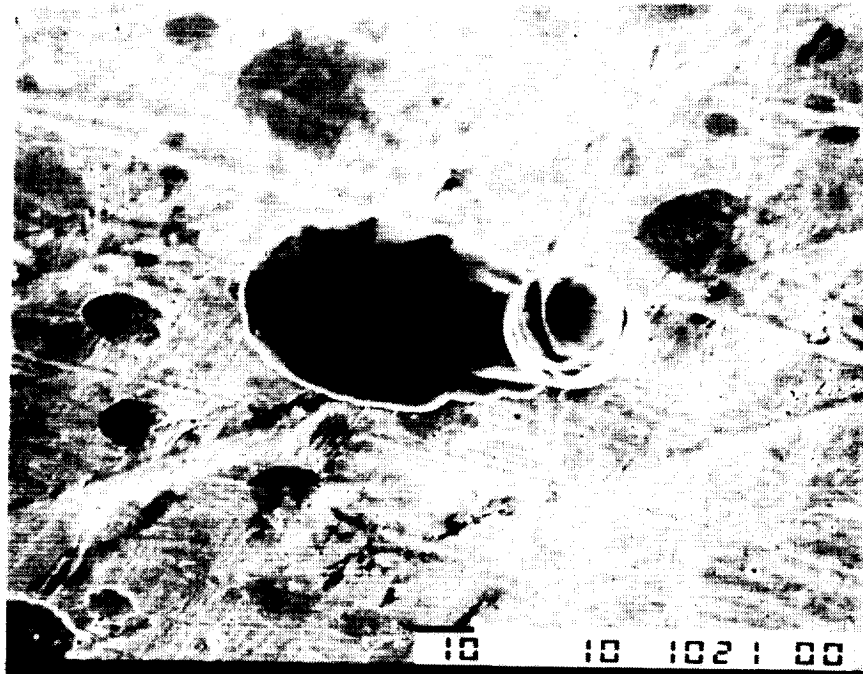
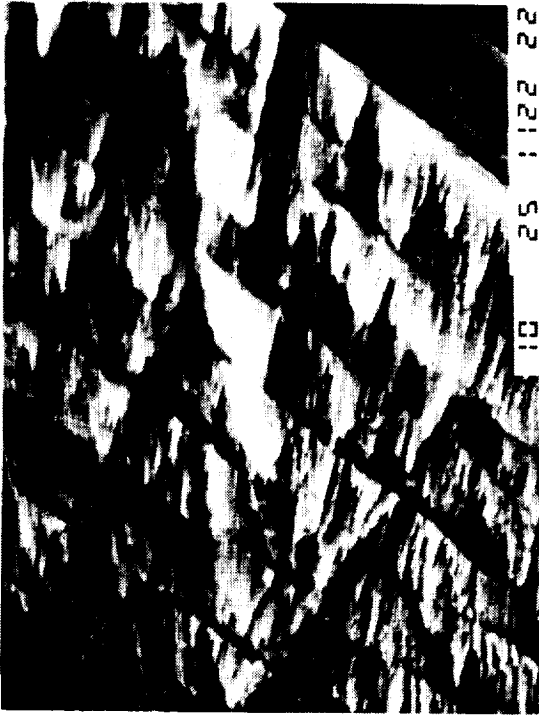


Fig. 16 Aluminum Ejecta Particles with Associated Splash Patterns

ORIGINAL PAGE  
BLACK AND WHITE PHOTOGRAPH



Impact Hole - Exposed Surface  
(x100)

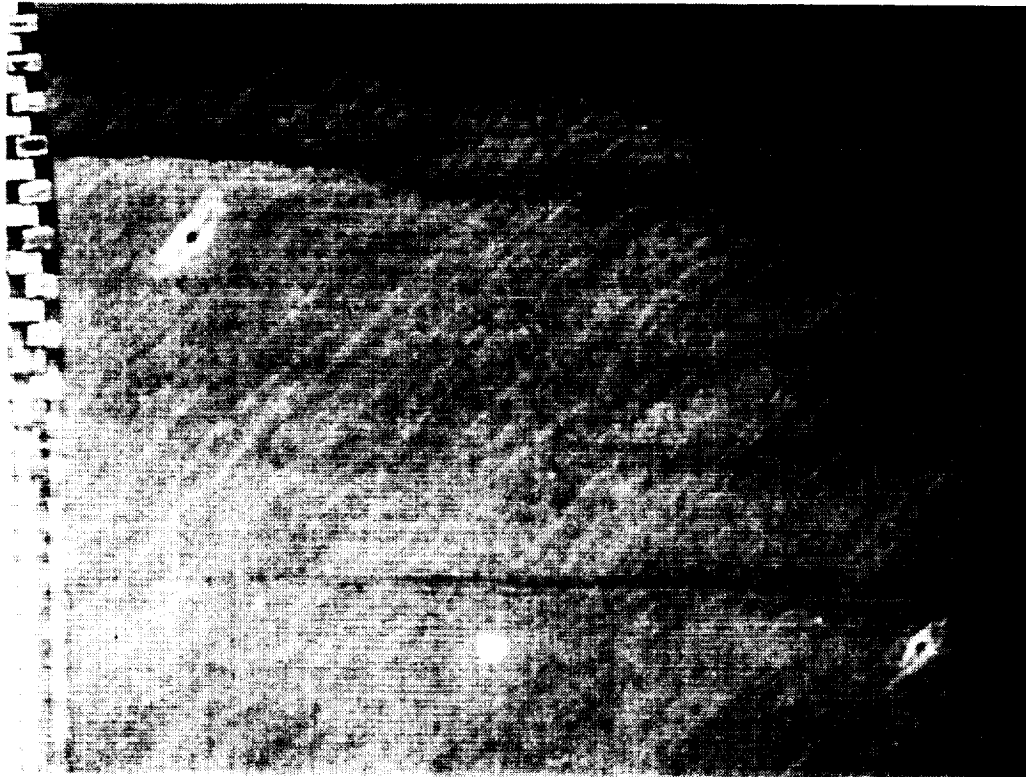
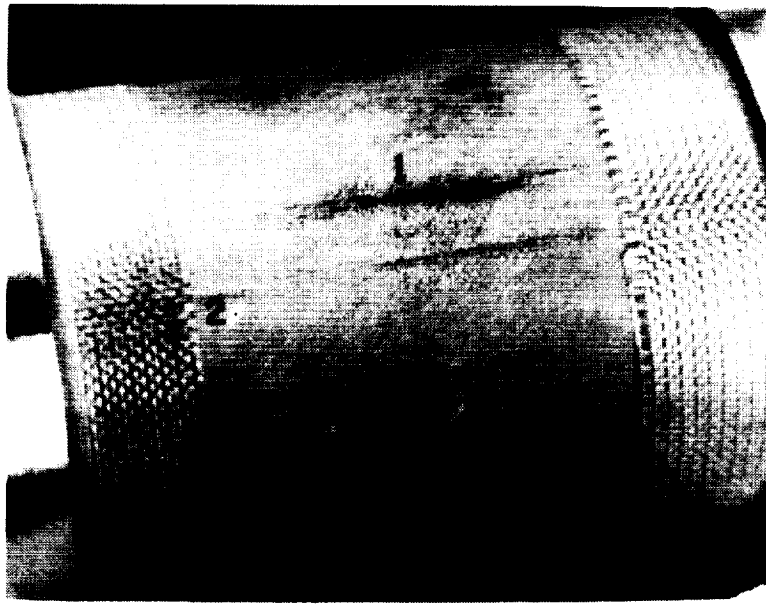


AO Erosion Morphology  
(x1500)



Exit Hole on  
Inside Tube Wall  
(x75)

Fig. 17 SEM Photographs of Micrometeoroid/Debris Impact/Exit Holes and AO Erosion Morphology for Graphite/Epoxy Tube [SP-288/T300, ( $\pm 43^\circ$ )<sub>4S</sub>]



(x5)

Fig. 18 Micrometeoroid/Debris Impacts on Kevlar®/Epoxy Tube [SP-328, ( $\pm 45^\circ$ )<sub>4S</sub>]



1



2

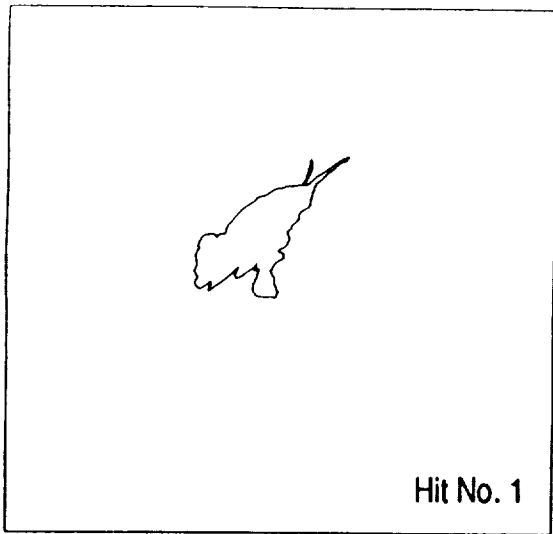


3



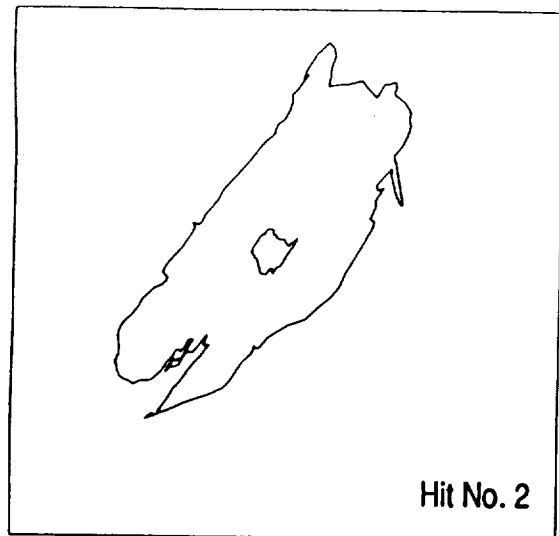
4

Fig. 19 Micrometeoroid/Debris Impact Damage (x100) on Kevlar®/Epoxy Tube [SP-328,  $(\pm 45^\circ)_{4S}$ ]



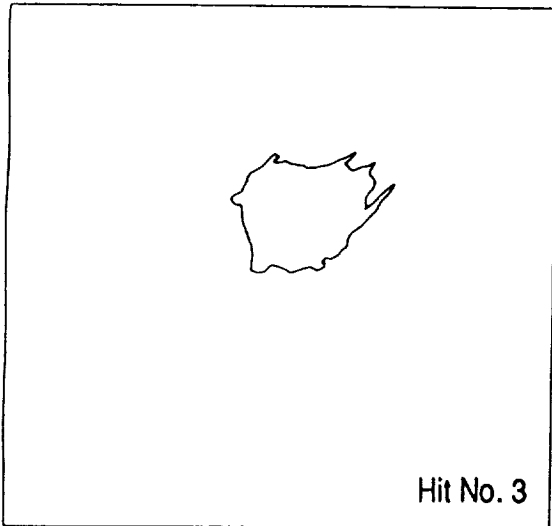
Hit No. 1

Surface Damage Area = 0.223 mm<sup>2</sup>  
Extent of Penetration = 1 - 2 plies



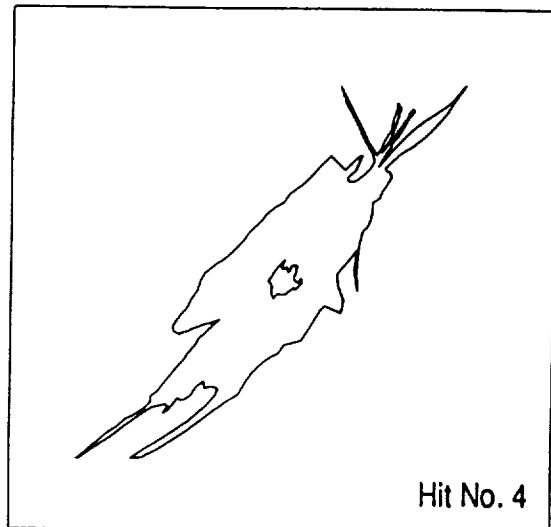
Hit No. 2

Surface Damage Area = 1.445 mm<sup>2</sup>  
Crater Area = 0.033 mm<sup>2</sup>  
Crater Diameter = 0.204 mm  
Extent of Penetration = 2 - 3 plies



Hit No. 3

Surface Damage Area = 0.370 mm<sup>2</sup>  
Extent of Penetration = 0 - 1 plies



Hit No. 4

Surface Damage Area = 0.881 mm<sup>2</sup>  
Crater Area = 0.020 mm<sup>2</sup>  
Crater Diameter = 0.159 mm  
Extent of Penetration = 2 - 3 plies

Fig. 20 Micrometeoroid/Debris Impact Damage SP328 Kevlar®/Epoxy Tube (2T17)